SUPPLEMENTAL DISCUSSION

Estimates for pK_a values

Accurate calculation of pK_a values is a computationally very challenging task. Here we use a fast heuristic scheme as implemented in PROPKA 3.1 (Søndergaard et al., 2011) to semi-quantitatively estimate the pK_a values of the conserved residues Asp133, Asp163, Asp164, and Lys300. Although not necessarily exact, the pK_a estimates are nevertheless thought to report on the chemical environment around titratable residues, and in particular, relative changes in the chemical environment will be reflected in shifts in the pK_a that are at least qualitatively indicative of likely protonation-state changes. pK_a values were calculated from frames of all MD trajectories at 1-ns intervals. PROPKA 3.1 can take ligands into account, so any Na$^+$ ion within 6 Å of the protein was included in the calculation. The resulting time series (Fig. S8, B–D) shows fluctuations >2–3 pK_a units, which indicates that the pK_a is sensitive to the exact molecular conformation. However, in aggregate, a more consistent picture emerges, as shown by the distributions of pK_a values (Fig. S9). When the data are grouped by the state of the Asp163–Lys300 salt bridge (for distance <4 Å, the salt bridge is considered formed or intact, whereas at ≥4 Å, it is considered broken; see Fig. S8 A), the effect of the salt bridge on the pK_a becomes apparent. In general, breakage of the salt bridge reduces the pK_a of Lys300 and raises the pK_a of Asp163. These are predicted to be around 10.5 and 4, respectively, when the salt bridge is intact. The pK_a of Asp164 is predicted to be in the range of 6 to 10 (Fig. S9), with the high values only appearing in simulations S1 (Fig. S9 A), when the solvent accessibility of Asp164 is decreased compared with the other simulations (Fig. S3, M–O). The pK_a of Asp133 is typically shifted down, but this is unlikely to have any substantial effect within the normal operating range of NhaA (pH 6.5–8.5) because the pK_a of Asp133 with the salt bridge intact is already around 5.

These absolute pK_a estimates have a high level of uncertainty. Relative changes, however, might be a better indicator for the effect of changes in the chemical environment of a titratable residue. We therefore focus on the shift in pK_a when the salt bridge is broken, ΔpK_a. The distribution of ΔpK_a is calculated from the pK_a distributions with and without the salt bridge (see Materials and methods in the main text) and is shown in Fig. S10. The means and standard deviations of these distributions allow for quick comparisons between different states (see Table 3 in the main text). The effect of the

salt bridge is clearly strongest for Lys300. The loss of the negatively charged carboxylate moiety of Asp163 reduces the pK_a of Lys300 by around 2 units (see Table 3, in particular simulations S2 and S4). It is the only residue for which the difference distribution (over all MD simulations) differs from 0 (i.e., no effect) by more than one standard deviation, indicating a significant stabilizing influence of the salt bridge on the charge state of Lys300. With a base pK_a on the order of 10.5 when the salt bridge is intact, such a shift brings Lys300 within the operating pH range of NhaA. Asp163 is shifted upwards but to a lesser degree (around 1.5 units), and because its base pK_a is low (~4), such a shift is less likely to result in a protonation-state change. Repeating the pK_a calculations while ignoring all sodium ions in the calculation showed that Asp163 is the only residue whose charge state appears to be substantially stabilized by a Na$^+$ ion (by about -0.9) when all data are considered in aggregate (see Table 3 in the main text); for all the other residues, the difference to the calculation including Na$^+$ was ≤0.3.

Sensitivity of the pK_a calculations

The effect of including Na$^+$ ions in the calculation was important, as shown by a stabilization of Asp163 by ~0.9; analysis of individual snapshots showed that a Na$^+$ ion could contribute up to 2 pK_a units. (Cl$^-$ ions were never close to the residues of interest and could be excluded.) The calculations were insensitive to using a slightly different criterion for the salt-bridge existence (a cutoff of 3.5 Å instead of 4 Å, as chosen in Fig. S8 A), which resulted in a difference of 0.1 or less (Table 3 in the main text). Similarly, changing the surface (or solvent) dielectric constant $\varepsilon_{surface}$ from its default value of 160 in the standard PROPKA 3.1 parametrization to a value of 80 only had a very small effect of ≤0.3, as seen in Table 3 in the main text. The change in the dielectric constant was motivated by the suggestion that ensembles of structures derived by NMR (and by extension, MD) might show fewer surface salt bridges, and thus a lower $\varepsilon_{surface}$, more similar to the solvent dielectric constant, might be appropriate to evaluate the Coulomb contribution to the pK_a (Søndergaard et al., 2011).

In summary, the calculated distributions of pK_a values are robust against relatively drastic parameter changes, as long as ions are explicitly take into account. The absolute accuracy of these values will be assessed by more sophisticated approaches in the future.

Movies from MD simulations

The first 250 ns of the 1-µs MD simulation trajectory S2/1 is shown in Videos 1 and 2. The coordinates were processed with a low-pass filter that removes rapid motions on the sub-ns timescale using the Gromacs tool *g_filter*. The simulations were performed with explicit solvent and membrane, but solvent, membrane, and all ions except for an ion participating in a binding event were omitted for clarity.
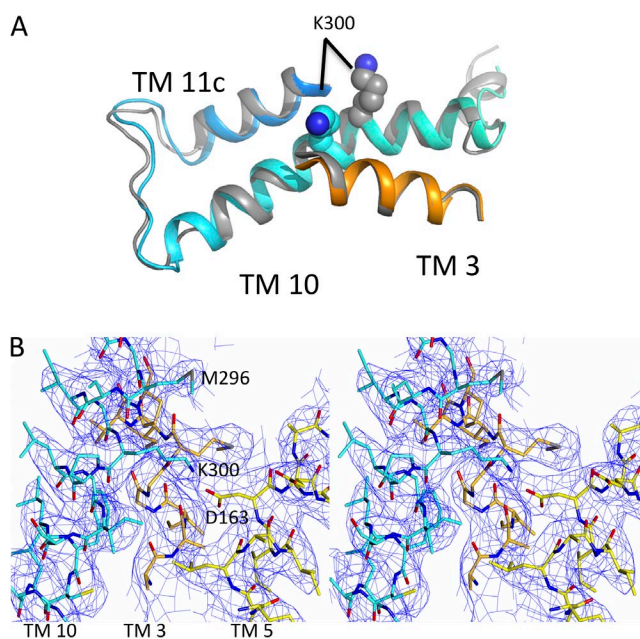

Figure S1. Sequence assignment of TM 10. (A) Superposition of TM 10 in cyan from the wild-type dimer structure on that of the same region from the published monomeric structure (gray; Hunte et al., 2005). The superposition was performed over all Cα atoms of the protomer. The Cα atom of Lys300 is displaced by one turn of the helix between the two structures. (B) Stereo diagram showing the 2mFo-DFc density associated with the refined structure of the triple mutant in the region of TM 10 and the Lys300–Asp163 salt bridge. TM 3 has orange carbon atoms, TM 5 has yellow, and TM 10 has cyan.
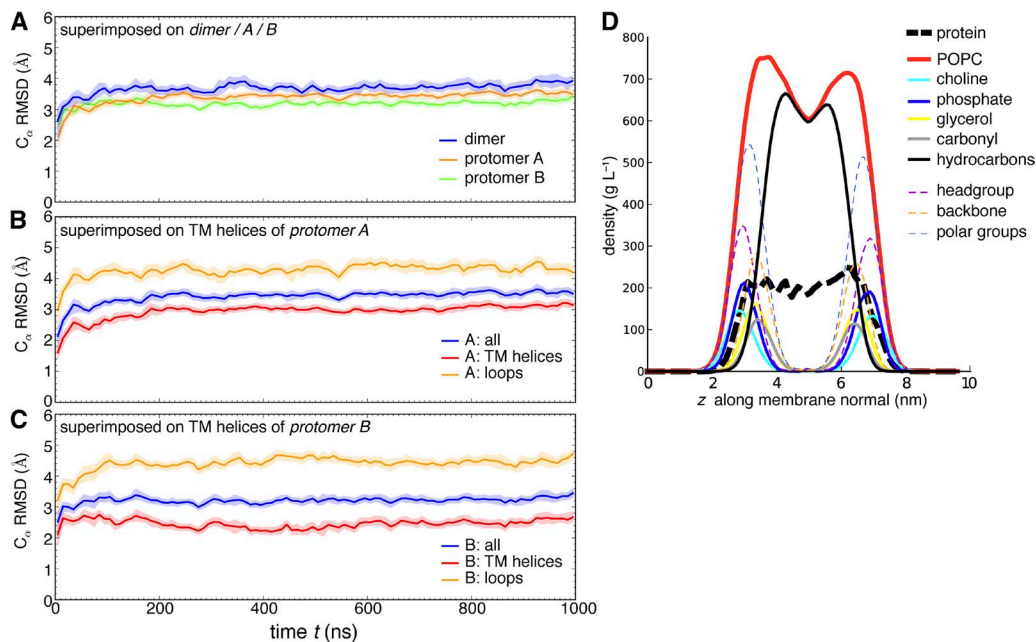
Figure S2. Analysis of proteins and lipids in a 1-μs simulation of the dimer (simulation S2/1). (A–C) RMSD of the NhaA dimer in membrane bilayer simulations. The coordinate root-mean-square distance of protein Cα atoms from the crystal structure was plotted as a function of time. Light bands indicate fluctuations between the 5th and 95th percentile around the average. (A) Blue, the dimer was superimposed on the crystal structure, and the RMSD was calculated for the whole dimer; orange, RMSD for protomer A only (superimposed on protomer A of the crystal structure); green, protomer B only. (B) RMSD of components of protomer A: blue, the whole protomer; red, only the TM helices (as defined by Hunte et al., 2005); orange, only the loops between the TM helices for protomer A superimposed on the TM helices. (C) RMSD of components of protomer B. (D) Lipid–protein density profile from MD simulation. The whole system was centered on the membrane. The density for components of the system was computed as averages in the plane of the membrane along the membrane normal z in 100 slices of thickness $\Delta z = 0.093$ nm. The periplasmic leaflet is marked by the peak around $z = 3$ nm, and the cytosolic leaflet is located at ∼6.5 nm. The protein is embedded in the membrane with the surfaces of NhaA lying inside the lipid head group region of the membrane. The graphs for protein and POPC are the totals for each group of molecules. Each POPC lipid molecule contains polar groups and the hydrocarbon core. Polar groups consist of the head groups (choline, phosphate) and the backbone (glycerol, carbonyl). Data for S2/1 are typical for other simulations not shown here.
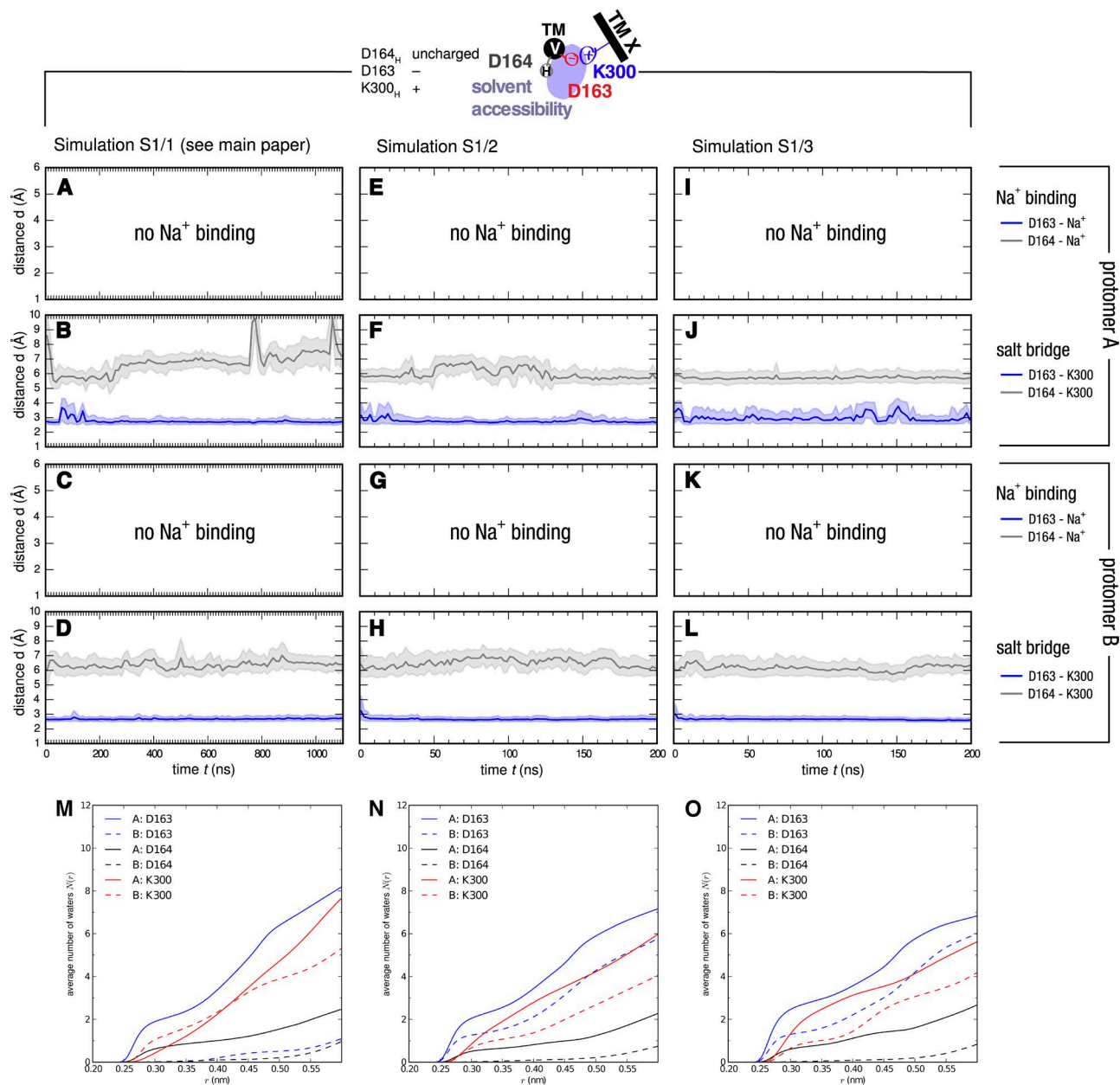
Figure S3. Analysis of simulations S1 (charged Asp163, neutral Asp164, charged Lys300). Results are shown for each protomer (labeled A and B). (Top; A–L) Distances between sodium ions and aspartate oxygen atoms (no binding observed in any simulations) and salt-bridge distances between Lys300, Asp163, and Asp164. (Bottom; M–O) Solvent accessibility of Asp163, Asp164, and Lys300, measured as the average number of water molecules as a function of distance from the aspartate carboxyl oxygens or the lysine amine nitrogen. Cartoon images illustrate the key characteristics observed in the simulations.
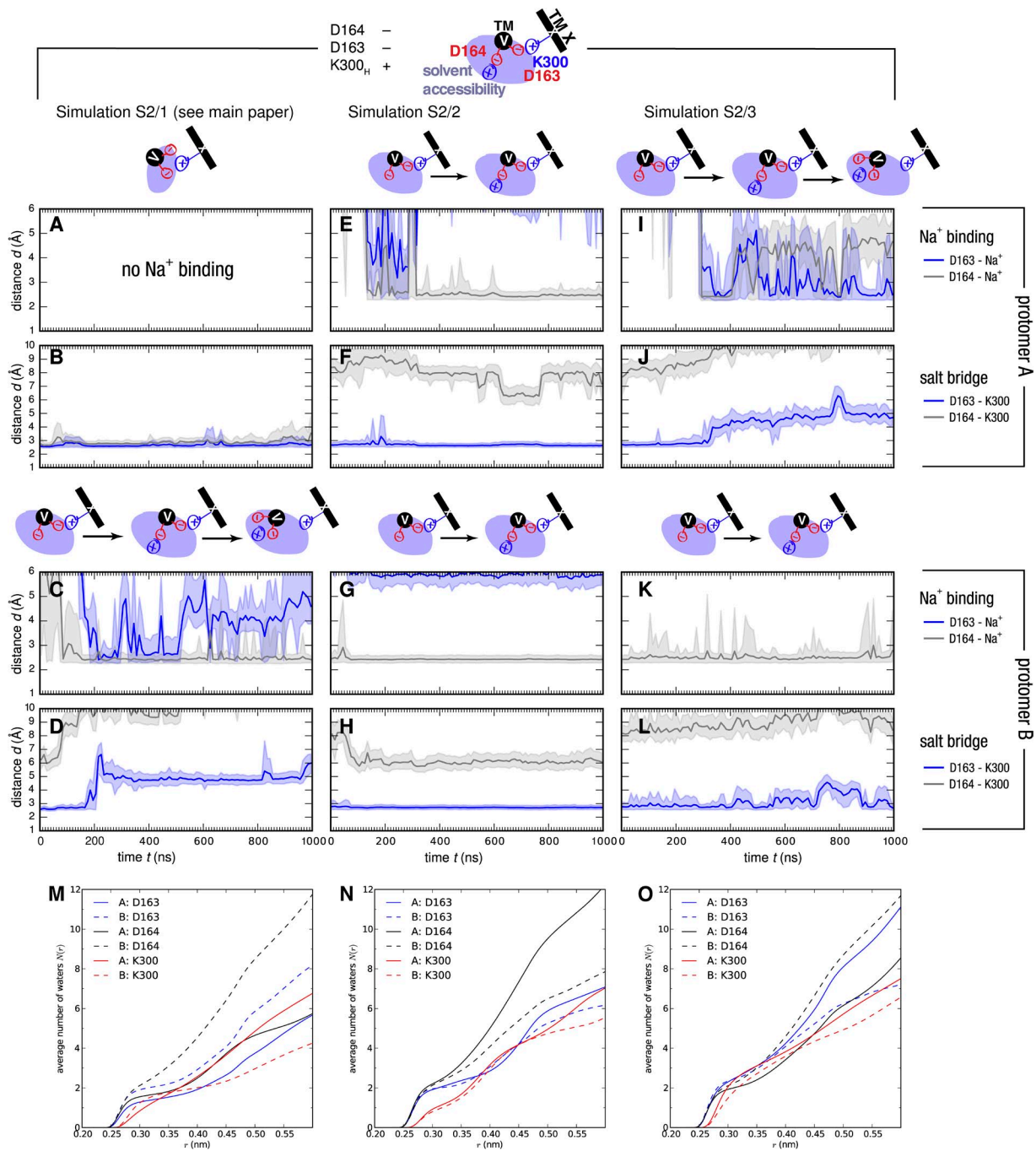
Figure S4. Analysis of simulations S2 (charged Asp163, charged Asp164, charged Lys300). Results are shown for each protomer (labeled A and B). Simulation S2/1 (protomer B) is also described in the main text and repeated here for convenience. (Top; A–L) Distances between sodium ions and aspartate oxygen atoms and salt-bridge distances between Lys300, Asp163, and Asp164. (Bottom; M–O) Solvent accessibility of Asp163, Asp164, and Lys300, measured as the average number of water molecules as a function of distance from the aspartate carboxyl oxygens or the lysine amine nitrogen. Cartoon images illustrate the key characteristics observed in the simulations.
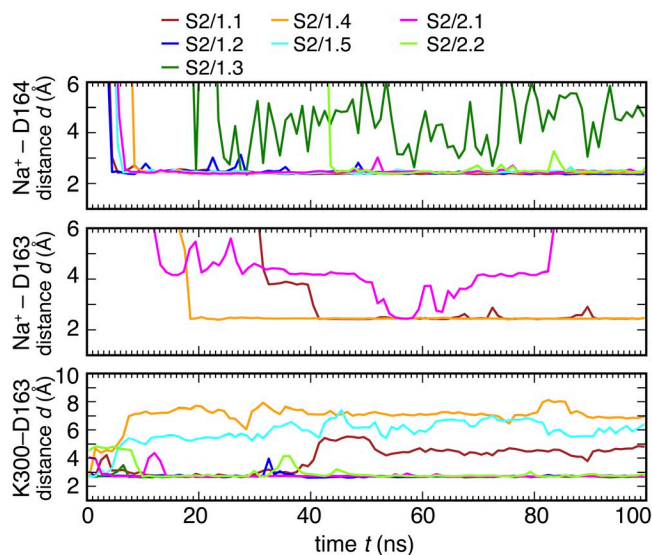
Figure S5. Monomer repeat simulations S2 (charged Asp163, charged Asp164, charged Lys300). Seven repeat simulations of the monomer system were analyzed in the same way as the dimer simulation (see Fig. S4 for details). Time series data were averaged in windows of length of 1 ns; fluctuations are not shown but are of similar magnitude as those in Fig. S4. (Top) Closest distance between a sodium ion and the δ-carboxyl oxygens of Asp164. A sodium ion binds to Asp164 in six of the repeats. In repeat 1.3, an ion enters the vestibule and stays in the vicinity of Asp164 but has not bound tightly by the end of the 100-ns simulation. (Middle) Closest distance between a sodium ion and Asp163. The broken Lys300–Asp163 salt bridge does not reform once a sodium ion is bound to Asp164 (repeat 1.5) or Asp164 and Asp163 (repeat simulations 1.1 and 1.4). The ion is not seen to bind to both Asp164 and Asp163 while the salt bridge is intact. (Bottom) Salt-bridge distance Lys300–Asp163. The salt bridge eventually breaks in three out of seven repeats (1.1, 1.4, and 1.5).
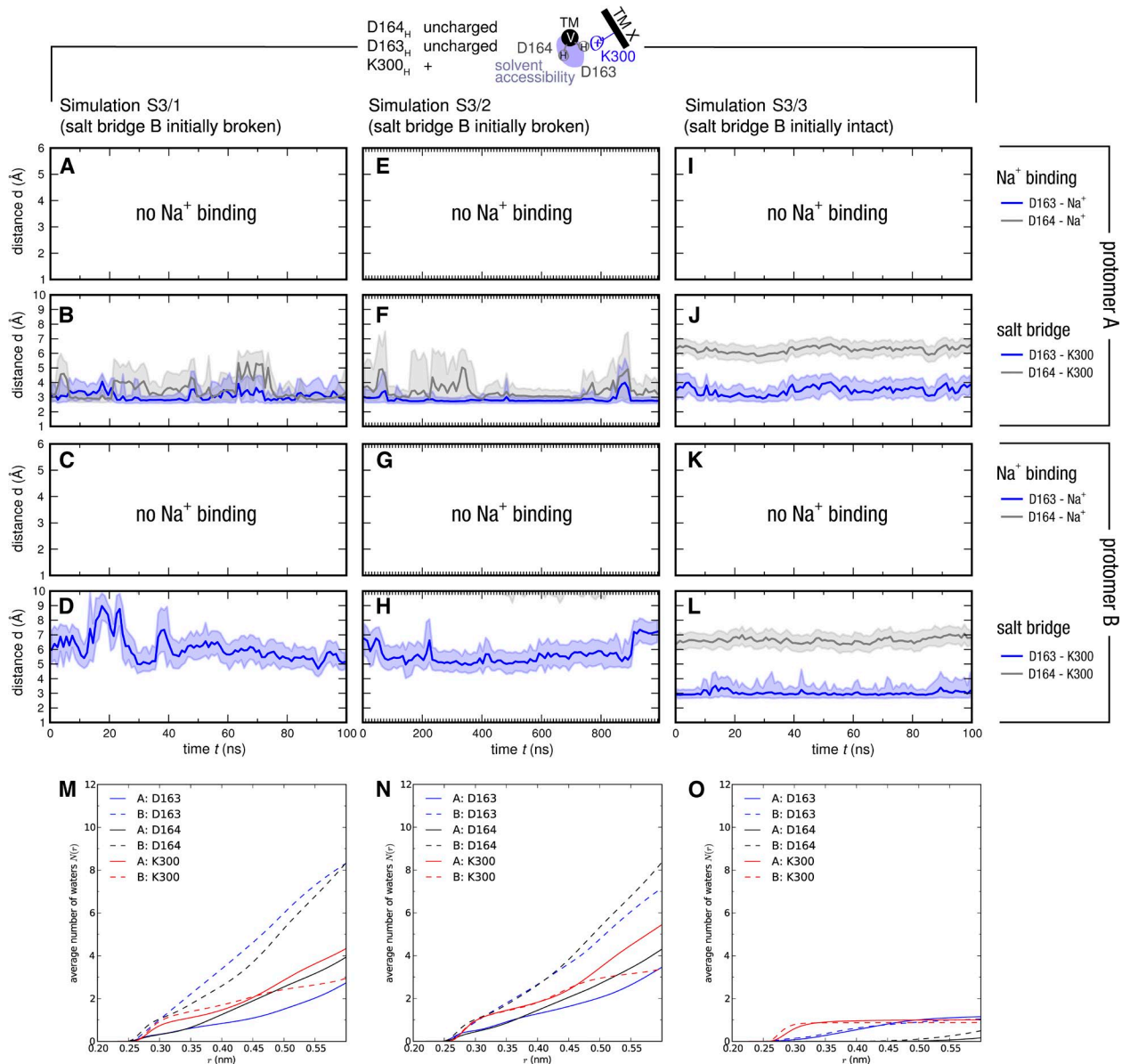
Figure S6. Analysis of simulations S3 (neutral Asp163, neutral Asp164, charged Lys300): Results are shown for each protomer (labeled A and B). Simulations S3/1 and S3/2 were initialized from configurations in which the salt bridge in protomer B was already broken (see Table 1 in the main text), whereas S3/3 had the salt bridges in both protomer A and B intact. (Top; A–L) Distances between sodium ions and aspartate oxygen atoms and salt-bridge distances between Lys300 (K300), Asp163 (D163), and Asp164 (D164). (Bottom; M–O) Solvent accessibility of Asp163, Asp164, and Lys300, measured as the average number of water molecules as a function of distance from the aspartate carboxyl oxygens or the lysine amine nitrogen. Cartoon images illustrate the key characteristics observed in the simulations.
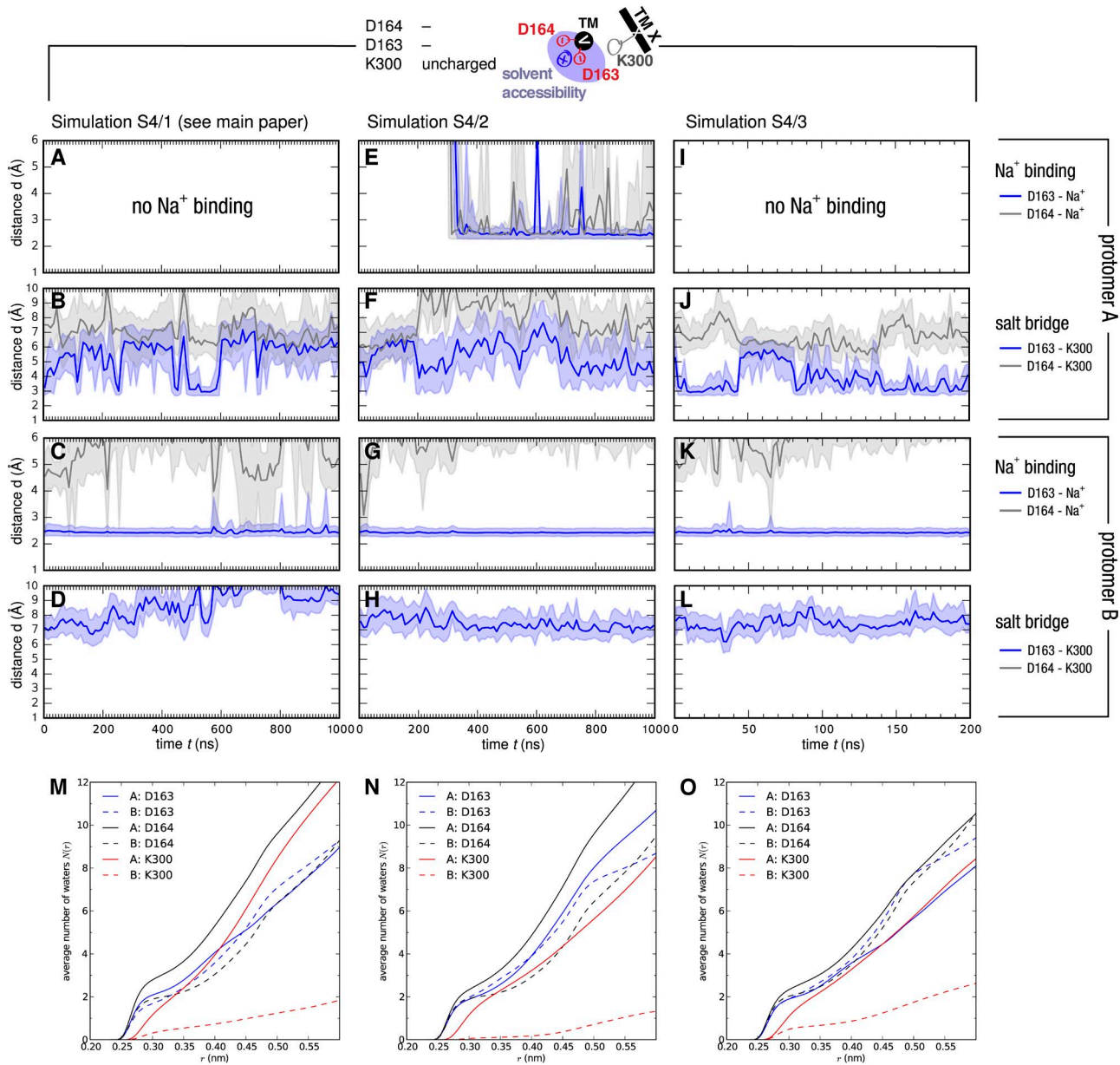
Figure S7. Analysis of simulations S4 (charged Asp163, charged Asp164, neutral Lys300). Results are shown for each protomer (labeled A and B). (Top; A–L) Distances between sodium ions and aspartate oxygen atoms and salt-bridge distances between Lys300 (K300), Asp163 (D163), and Asp164 (D164). (Bottom; M–O) Solvent accessibility of Asp163, Asp164, and Lys300, measured as the average number of water molecules as a function of distance from the aspartate carboxyl oxygens or the lysine amine nitrogen. Cartoon images illustrate the key characteristics observed in the simulations.
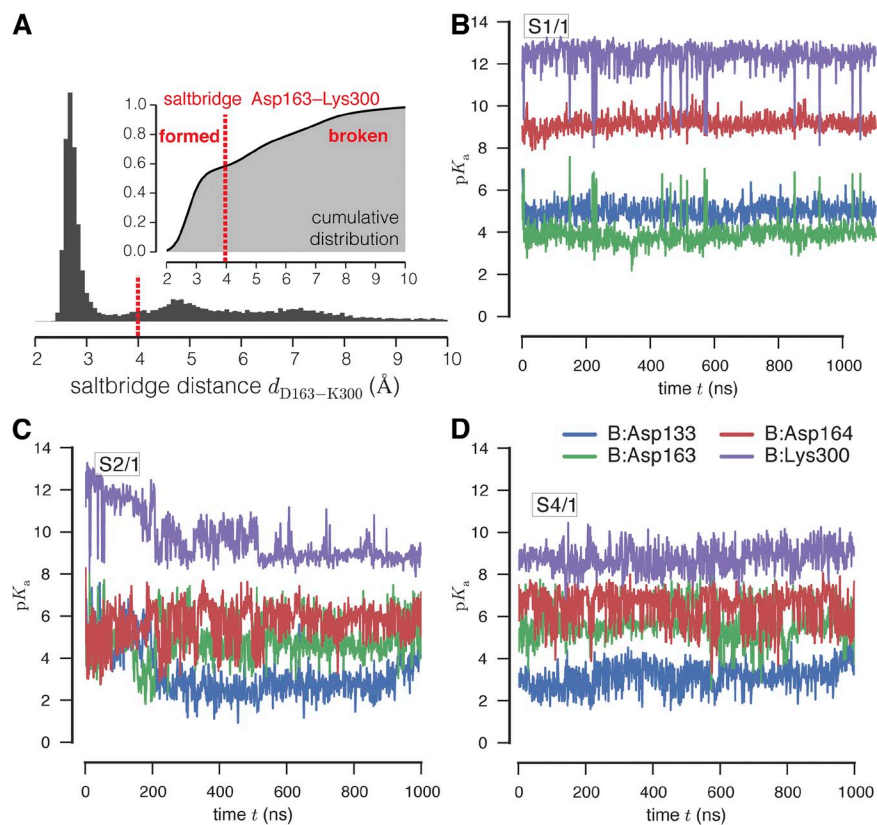
Figure S8. Raw data for pK_a value analysis. (A) Histogram of salt-bridge Asp163–Lys300 distances over all simulations. (Inset) Cumulative distribution. The salt bridge was considered formed for $d < 4$ Å and broken at ≥ 4 Å. All further analysis is fairly insensitive to the exact value because changing the cutoff by ± 0.5 Å only changes the number of included snapshots by less than $\sim 5\%$, as seen from the cumulative distribution. (See also Table 3 in the main text for supporting results from a sensitivity analysis.) (B) pK_a calculated by PROPKA 3.1 for frames sampled every 1 ns from the S1/1 trajectory, protomer B. No ion binding occurs, and the salt bridge remains intact. (C) S2/1 simulation, protomer B. Ion binding to Asp164 occurs between 20 and 100 ns, and the salt bridge breaks around 200 ns, resulting in a decrease in the pK_a of Lys300. (D) S4/1 simulation, protomer B. The salt bridge remains broken with a Na$^+$ shared between Asp164 and Asp163.
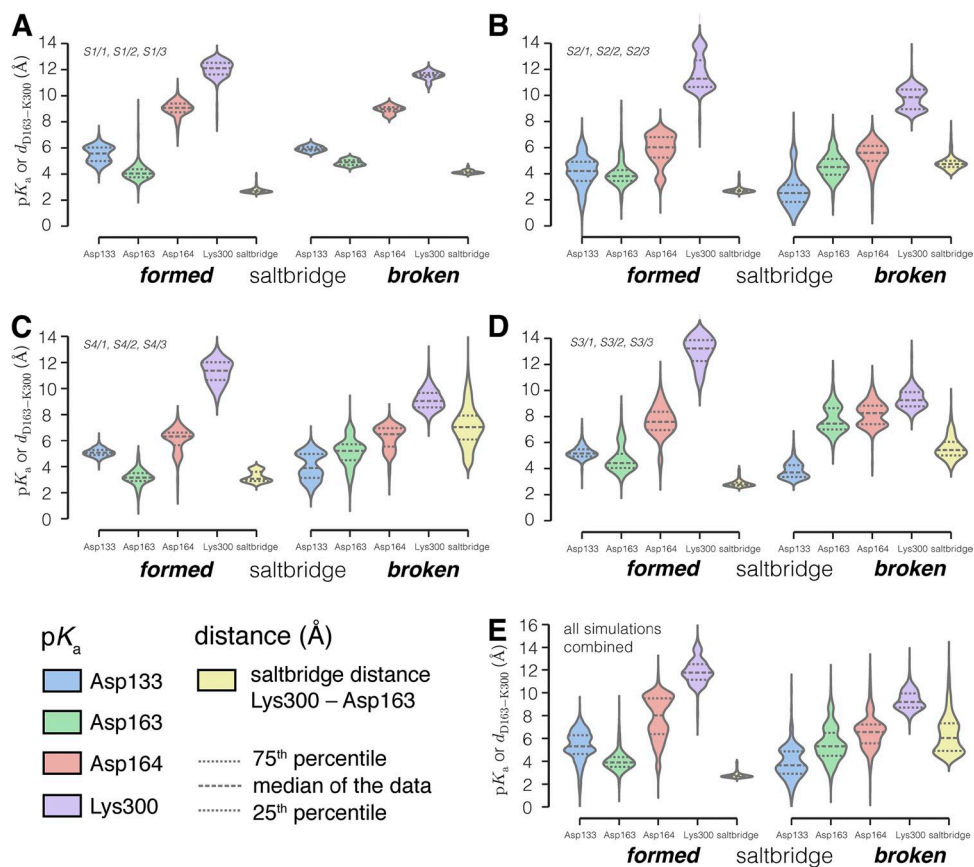
Figure S9. Analysis of pK_a values by simulation and salt-bridge state. Distributions of pK_a values are shown as violin plots for the four conserved residues of interest, grouped by (a) simulated protonation states and (b) state of the salt bridge (formed or broken). Distributions are scaled to have the same maximum width. The 25th, 50th (median), and 75th percentiles of the data are indicated by dashed lines. The distribution of the salt-bridge distance (yellow) is also included on the same scale (in Å) and can be seen to be <4 Å (formed) and ≥4 Å (broken). (A) Simulations S1 (Asp163 deprotonated and Asp164 and Lys300 protonated). (B) Simulations S2 (Asp163 and Asp164 deprotonated and Lys300 protonated). (C) Simulations S4 (Asp163, Asp164, and Lys300 deprotonated). (D) Simulations S3 (Asp163, Asp164, and Lys300 protonated). (E) Data from all simulations shown in Table 1 in the main text were combined and analyzed in aggregate.
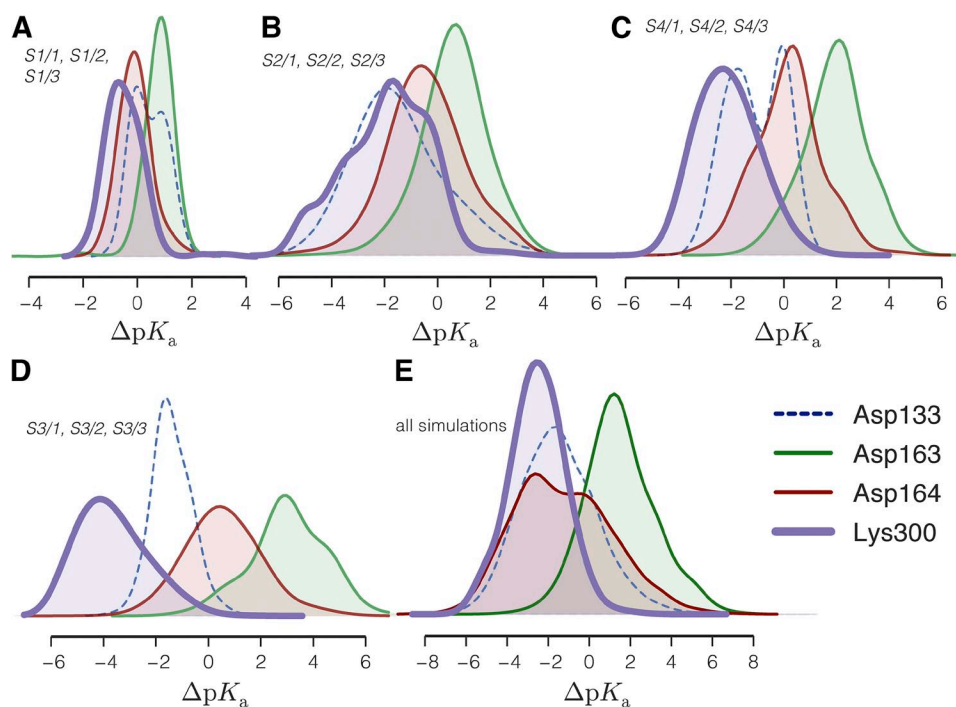
Figure S10. Shift in pK_a caused by breaking of the Asp163–Lys300 salt bridge. The distribution of the shift $\Delta \mathrm{p}K_a = \mathrm{p}K_a^{\text{salt bridge broken}} - \mathrm{p}K_a^{\text{salt bridge intact}}$ quantifies how the chemical environment around the titratable residues changes as a consequence of breaking the salt bridge (and concomitant Na$^+$ binding). (A) Simulations S1 (Asp163 deprotonated and Asp164 and Lys300 protonated). (B) Simulations S2 (Asp163 and Asp164 deprotonated and Lys300 protonated). (C) Simulations S4 (Asp163, Asp164, and Lys300 deprotonated). (D) Simulations S3 (Asp163, Asp164, and Lys300 protonated). (E) All simulations listed in Table 1 in the main text analyzed in aggregate.
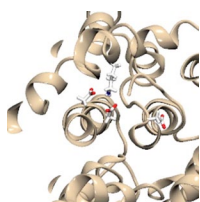
Video 1. NhaA, protomer A, 0–250 ns from simulation S2/1. Stable salt-bridge network between Lys300 and Asp163/Asp164. The conformation of the network is essentially unchanged over the course of the whole simulation, and hence only the first 250 ns are shown.
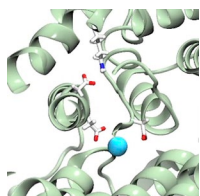
Video 2. NhaA, protomer B, 0–250 ns from simulation S2/1. A sodium ion spontaneously binds to Asp133 and Asp164. Asp133 moves away, leaving the ion with Asp164. The salt bridge Lys300–Asp163 breaks and Asp163 binds the Na$^+$ ion together with Asp164, preventing the reformation of the salt bridge. These interactions remain until the end of the 1-μs simulation, even though only the first 250 ns are shown.

Table S1

Solubilization efficiency of NhaA constructs

Detergent solubilization efficiency in 2% (wt/vol) OG	Number of NhaA constructs
10–20%	20[a]
20–30%	17
30–40%	6
>50%	2

[a]Extraction efficiency of wild-type NhaA is between 10 and 20% in 2% OG.

Table S2

RMSD in positions of C_α atoms among the structures

Chain	Monomer				Dimer	
	Chain B	Chain C	Chain D	1ZCD[a]	Dimer CD	1FI1[b]
Chain A[c]	0.3	0.0	0.3	1.0 358/374[d]	—	—
Dimer AB	—			—	0.3	1.2 702/752[d]

[a]Previously published monomeric x-ray structure (Hunte et al., 2005).
[b]Model from Cryo-EM (Appel et al., 2009).
[c]NhaA triple mutant.
[d]*n/m: n* residues out of *m* residues matched using the algorithm as described in Materials and methods in the main text.

REFERENCES

Appel, M., D. Hizlan, K.R. Vinothkumar, C. Ziegler, and W. Kühlbrandt. 2009. Conformations of NhaA, the Na^+/H^+ exchanger from *Escherichia coli*, in the pH-activated and ion-translocating states. *J. Mol. Biol.* 388:659–672. http://dx.doi.org/10.1016/j.jmb.2009.03.010

Hunte, C., E. Screpanti, M. Venturi, A. Rimon, E. Padan, and H. Michel. 2005. Structure of a Na^+/H^+ antiporter and insights into mechanism of action and regulation by pH. *Nature.* 435:1197–1202. http://dx.doi.org/10.1038/nature03692

Søndergaard, C.R., M.H.M. Olsson, M. Rostkowski, and J.H. Jensen. 2011. Improved treatment of ligands and coupling effects in empirical calculation and rationalization of pKa values. *J. Chem. Theory Comput.* 7:2284–2295. http://dx.doi.org/10.1021/ct200133y